

ENERGY-DEPENDENT CROSS SECTIONS FOR K^- NEUTRON INTERACTIONS IN THE CM ENERGY RANGE 1750–2200 MeV FROM FIVE K^- DEUTERIUM BUBBLE CHAMBER EXPERIMENTS

M.J. CORDEN, G.F. COX, A. DARTNELL, I.R. KENYON, S.W. O'NEALE,
K.C.T.O. SUMOROK, J.A. STUBBS, P.M. WATKINS

Department of Physics, University of Birmingham

Received 20 June 1977

Experimental details and channel cross sections are presented for five K^- deuterium bubble chamber experiments. Utilising the Fermi motion of the neutron the K^-n cross sections are extracted over the c.m. energy range 1750–2200 MeV and where possible results are compared to related channels from other experiments.

1. Introduction

This paper presents the K^- neutron cross sections of all the major reactions studied in five K^- deuterium bubble chamber experiments at incident momenta of 1130, 1320, 1450, 1650 and 1780 MeV/c. Because of the Fermi motion of the target neutron these experiments span the c.m. energy region 1750–2200 MeV. This is the only K^- deuterium bubble chamber data in the range 1900–2200 MeV. The K^- neutron initial state is a pure isospin one, and so these data should provide a useful constraint for analyses of mixed isospin states from K^-p experiments in this energy region where the Σ resonance spectrum is still uncertain.

This paper begins with a discussion of those scanning and processing procedures which are common to all the reactions. The weighting and treatment of ambiguities are discussed for each reaction and the channel cross sections for each of the experiments are quoted. Finally, the energy-dependent cross sections of all the major reactions are presented and, where possible, these are compared with the results of related experiments.

2. Experimental procedure

2.1. General

The experiments with K^- incident momenta of 1450 and 1650 MeV/c together involved 700 K pictures and were performed using the Saclay 80 cm bubble cham-

ber by a collaboration of Birmingham, Edinburgh and Glasgow universities and Imperial College, London. Details of the scanning and processing for these experiments are presented elsewhere [1]. The experiments at incident K^- momenta of 1130, 1320 and 1780 MeV/c used the CERN 2m bubble chamber and involved 220 K, 110 K and 150 K pictures respectively. These experiments were scanned and measured at Birmingham. In the later sections the experiments will be referred to as experiments 1 to 5 in order of increasing incident momentum.

2.2. Scanning

The film was scanned for all events with an odd number of outgoing tracks or with a visible slow proton (a dark track less than 20 cm long), except those with only one or two outgoing charged tracks and with no observed charged or neutral decays. These criteria isolate K^- neutron interactions where the proton from the deuteron acts as a spectator. The events were scanned and predigitised for an HPD measurement and a 10% rescan was performed to evaluate scanning efficiencies. These are listed for each experiment as a function of event topology in table 1. A special rescan was performed for experiment 5, for events with a neutral decay pointing to a vertex where the angle between the outgoing track and the incident beam was small. This was done to improve the low scanning efficiency for this type of event in this experiment.

2.3. Processing

All events from experiments 1, 2 and 5 were measured on the Birmingham University Film Analysis Group's HPD and events failing geometrical reconstruction on the first pass were remeasured. Events that were considered unsatisfactory after

Table 1
Efficiency of a single scan as a function of topology for experiments 1, 2 and 5

Topology code	Experiment 1 (1130 MeV/c)	Experiment 2 (1320 MeV/c)	Experiment 5 (1780 MeV/c)
101, 201	0.829 ± 0.015	0.832 ± 0.013	0.817 ± 0.012
210	0.800 ± 0.015	0.765 ± 0.016	0.782 ± 0.015
300, 400, 301, 401	0.855 ± 0.020	0.850 ± 0.017	0.808 ± 0.020
310, 410	0.822 ± 0.028	0.884 ± 0.018	0.785 ± 0.021

For each three-digit topology code xyz , x is the total number of outgoing charged tracks at the primary vertex, y is the number of charged decays (kinks), and z is the number of neutral decays (vees)

kinematic fitting were also remeasured. There were two separate remeasurements of the failed events from experiment 5. The events were analysed using modified versions of the Rutherford Laboratory geometrical reconstruction and kinematic fitting programmes.

When available the ionisation measurements from the HPD were used in the fit selection, and all fitted events where the ionisation measurements were incomplete were checked on the film by physicists. This was particularly important for the short Σ^- decays where the HPD frequently failed to obtain a satisfactory ionisation measurement. A complete list of the reactions to be described in this paper is presented in table 2. Probability cuts of 1% (5%) were used in the selection of four (one) constraint production vertex fits for further analysis.

2.4. Spectator protons

Approximately one third of the K^- neutron interactions observed in a deuterium bubble chamber have a visible spectator proton and these events are processed in the standard manner. When the spectator proton from the deuteron was not visible (unseen spectator), fits were made by inserting at the production vertex a proton with momentum components $P_x = P_y = P_z = 0$ and external errors $\Delta P_x = \Delta P_y = \frac{3}{4} \Delta P_z = 30 \text{ MeV}/c$. This procedure works well when the spectator is the only missing particle in the final state, yielding fitted quantities slightly more accurately than a one constraint fit made without the additional constraints. The momentum distribution of the spectator proton for this type of reaction is consistent with that calculated assuming a Hulthén wave function for the deuteron. This is illustrated for reaction (6) from experiment 2 in fig. 1a.

When there is an additional missing neutral particle in the final state the fitting

Table 2
List of reactions studied

$K^-d \rightarrow p_s \Lambda^0 \pi^-$	(1)
$K^-d \rightarrow p_s \Lambda^0 \pi^- \pi^0$	(2)
$K^-d \rightarrow p_s \Sigma^0 \pi^-$	(3)
$K^-d \rightarrow p_s \Lambda^0 \pi^- \pi^+ \pi^-$	(4)
$K^-d \rightarrow p_s \Sigma^0 \pi^- \pi^+ \pi^-$	(5)
$K^-d \rightarrow p_s K^- \pi^- p$	(6)
$K^-d \rightarrow p_s \bar{K}^0 \pi^- n$	(7)
$K^-d \rightarrow p_s \Sigma^- \pi^0$	(8)
$K^-d \rightarrow p_s \Sigma^- \pi^+ \pi^-$	(9)
$K^-d \rightarrow p_s \Sigma^+ \pi^- \pi^-; \Sigma^+ \rightarrow \pi^+ n$	(10a)
$K^-d \rightarrow p_s \Sigma^+ \pi^- \pi^-, \Sigma^+ \rightarrow \pi^0 p$	(10b)
$K^-d \rightarrow p_s \Sigma^- \pi^+ \pi^- \pi^0$	(11)
$K^-d \rightarrow p_s \Sigma^+ \pi^- \pi^- \pi^0, \Sigma^+ \rightarrow \pi^+ n$	(12a)
$K^-d \rightarrow p_s \Sigma^+ \pi^- \pi^- \pi^0, \Sigma^+ \rightarrow \pi^0 p$	(12b)

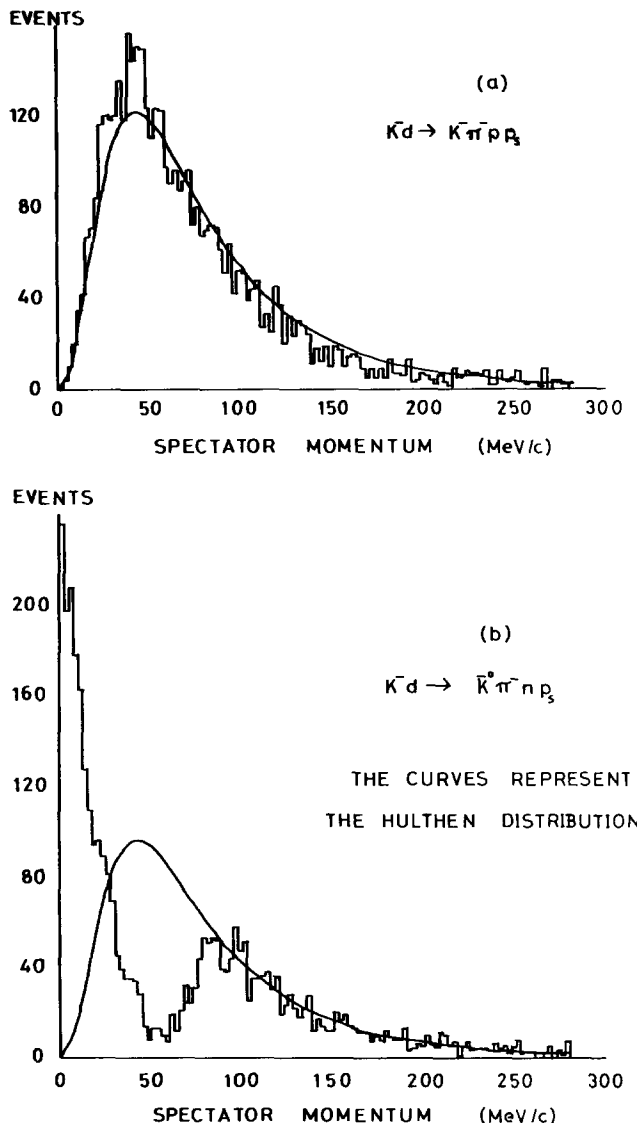


Fig. 1. Spectator momentum distribution for (a) reaction (6) in experiment 2 and (b) reaction (7) in experiment 2. The curves in both cases are the predictions of the Hulthén wave function

procedure leaves the starting values essentially unchanged for unseen spectators so that the true distribution is not reproduced. This is illustrated for the reaction (7) from experiment 2 in fig. 1b where it is clear that the fitted momentum of the unseen particle is biased and the interaction energy is less well determined.

In common with other experiments in deuterium [2], there is in all reactions an excess of events with spectator momentum above 280 MeV/c compared with the prediction of the Hulthén wave function. This could arise from interactions of the incident kaon with the deuteron as a whole or from interactions with a single nucleon where one of the secondary particles subsequently reacts with the other nucleon from the deuteron. In the absence of detailed knowledge of the mechanisms leading to fast spectator events an allowance for these effects was included in the cross section but, for analysis, events with a spectator momentum greater than 280 MeV/c were excluded. The procedure adopted for the selection of the spectator nucleon in reactions (6) and (7) (see table 2) where there are two nucleons in the final state is described in sect. 4.

2.5. Event weighting

For reactions involving a charged or neutral decay there are losses for decays which occur very close to the production vertex and for events where the decay is near the edge of or outside the visible region of the bubble chamber. These are corrected by applying uniform production and decay fiducial volume cuts to all the channels and by requiring a minimum projected length for the decay track. The remaining events are weighted by the factor W where

$$W = \left[\exp\left(\frac{-l_0}{L \cos \lambda}\right) - \exp\left(\frac{-l_p}{L}\right) \right]^{-1}.$$

L is the length of the decaying track, λ is its dip angle, l_p the potential visible path length for its decay and l_0 is the minimum projected decay length cutoff. The values used for l_0 in each channel are given in table 3a. These were obtained by maximising

Table 3a
Minimum projected decay lengths

Particle	Λ^0	K_s^0	Σ^-	Σ^+
Cutoff value (cm)	0.3	0.3	0.6	0.6

Table 3b
Selections which events ambiguous between Λ^0 and Σ^0 reactions must satisfy to be included in samples for further analysis (the Σ^0 decay angles α and β are defined in the text)

Λ^0 sample	Σ^0 sample
$\cos \alpha < -0.75$ $ \cos \beta < 0.5$	$\cos \alpha > 0$

the total weighted number of events as cuts were varied. Other weights that were only applied to certain channels are discussed in sects. 3 and 5.

2.6. Ambiguities

There are relatively few ambiguities in these low energy experiments. However, the Λ^0/Σ^0 ambiguity has to be resolved and reactions (2) and (8) (table 2) have to be isolated from an overlap with multi-neutral reactions. For the cross section determination only a statistical separation is necessary. For any analysis involving individual events it is necessary to apply more restrictive cuts to minimise the contamination of the channels. These separation procedures are described in sect. 3.

Where there are a small number of ambiguous fits for cross-section calculations these have been allocated to reactions in the same ratio as the unique fits. In the analysis of these channels ambiguous fits have been excluded except where they clearly populate a restricted kinematic region.

3. Λ^0 and Σ^0 channels

We discuss here those channels involving a Λ^0 or a Σ^0 , reactions (1) to (5) in table 2. The numbers of unique and ambiguous fits to these reactions are presented in table 4. There are some ambiguous fits between reactions (2) and (3) and in these cases we have chosen the most highly constrained fit. This separation was supported

Table 4
Raw numbers of unique and ambiguous fits for each channel for experiments 1, 2 and 5

Reaction	Experiment 1		Experiment 2		Experiment 5	
	unique	ambiguous	unique	ambiguous	unique	ambiguous
(1) $K^-d \rightarrow p_s \Lambda^0 \pi^-$	2281	3696	1433	1966	1214	2250
(2) $K^-d \rightarrow p_s \Lambda^0 \pi^- \pi^0$	6547	350	4952	278	6470	406
(3) $K^-d \rightarrow p_s \Sigma^0 \pi^-$	816	3983	501	2196	343	2533
(4) $K^-d \rightarrow p_s \Lambda^0 \pi^+ \pi^- \pi^-$	242	113	310	126	526	600
(5) $K^-d \rightarrow p_s \Sigma^0 \pi^+ \pi^- \pi^-$	28	113	48	131	109	635
(6) $K^-d \rightarrow p_s K^- \pi^- p$	2407	58	1976	169	4420	74
(7) $K^-d \rightarrow p_s \bar{K}^0 \pi^- n$	1471	0	1615	3	3953	17
(8) $K^-d \rightarrow p_s \Sigma^- \pi^0$	1026	24	635	22	1054	66
(9) $K^-d \rightarrow p_s \Sigma^- \pi^+ \pi^-$	1377	13	1369	5	1441	11
(10a) $K^-d \rightarrow p_s \Sigma^+ \pi^- \pi^-$	1100	10	912	8	750	9
(10b) $K^-d \rightarrow p_s \Sigma^+ p \pi^- \pi^-$	898	85	657	25	537	14
(11) $K^-d \rightarrow p_s \Sigma^- \pi^+ \pi^- \pi^0$	368	12	286	5	1132	47
(12a) $K^-d \rightarrow p_s \Sigma^+ \pi^- \pi^- \pi^0$	57	2	80	6	183	11
(12b) $K^-d \rightarrow p_s \Sigma^+ p \pi^- \pi^- \pi^0$	52	14	74	7	137	18

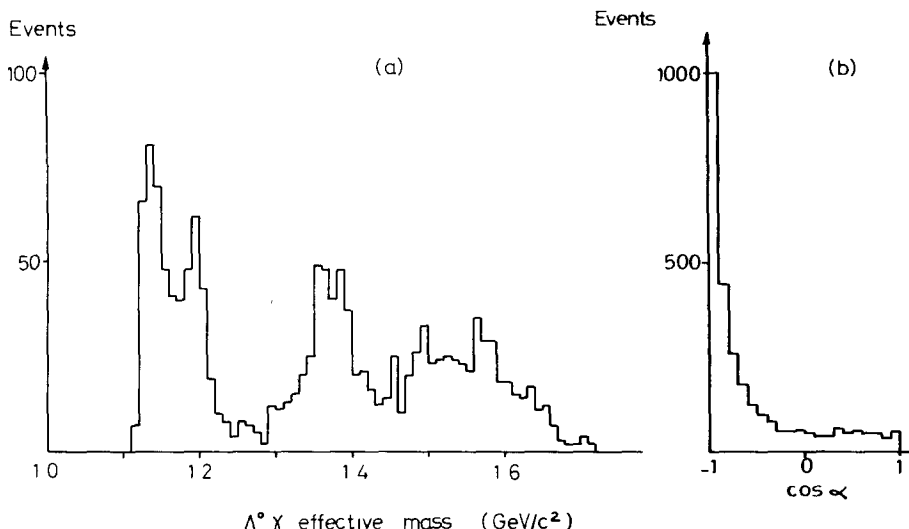


Fig. 2 (a) The $(\Lambda^0\gamma)$ effective mass distribution for a sample of $K^-d \rightarrow p_s\Lambda^0\gamma\pi^-\gamma$ fits (b) Distribution in $\cos\alpha$ for all fits to reaction (3), both unique and ambiguous, from experiment 1

by a study of the hypothesis $K^-d \rightarrow p_s\Lambda^0\pi^-\gamma$. The effective mass of the $(\Lambda^0\gamma)$ combination for experiment one is shown on fig. 2a where it is clear that reactions (1) and (3) are well separated from reaction (2). The ambiguity between reactions (1) and (3) has been treated in the usual way by studying the distribution of the angle α between the decay γ in the Σ^0 rest frame and the Σ^0 direction in the c.m. rest frame. For genuine Σ^0 decays this distribution should be isotropic, but when plotted for all Σ^0 fits it has a large peak near $\cos\alpha = -1$ due to Λ^0 events. This is illustrated in fig. 2(b) for events from experiment 5, which is the highest energy experiment.

The cross sections for the Λ^0 and Σ^0 channels were calculated as follows:

(a) The total number of genuine Σ^0 fits was determined by multiplying the number of events with $\cos\alpha > 0$ by two

(b) This number was subtracted from the total number of Λ^0 events giving either Λ^0 or Σ^0 fits to give the total number of genuine Λ^0 fits.

The selections used for the isolation of Λ^0 and Σ^0 samples for further analysis are given in table 3b. The angle β between the γ -ray and the production plane normal was also used in this selection as $\cos\beta$ tends towards zero for genuine Λ^0 events. The number of ambiguous events included in the Σ^0 analysis sample is very small, but ambiguous events make an important contribution to the Λ^0 analysis sample. The above procedure has also been followed for reactions (4) and (5).

Reaction (2) is also contaminated by events from the unconstrained $\Sigma^0\pi^-\pi^0p_s$ and $\Lambda^0\pi^-\pi^0\pi^0p_s$ final states. A spurious $\Lambda(1520)$ signal can be seen in the $\Lambda^0\pi^0$ mass plot for reaction (2) due to $\Lambda(1520)$ decays to $\Sigma^0\pi^0$ and $\Lambda^0\pi^0\pi^0$, where the low mass $\pi^0\gamma$ or $\pi^0\pi^0$ pair is misfitted as a single π^0 . No such effect is observed for

events having a χ^2 probability greater than 50% and a missing mass squared less than the π^0 mass squared, and corresponding cuts were used with the appropriate correction factors in the cross section determination. These cuts only produced significant changes in the calculated cross sections for the two highest energy experiments.

In addition to the event weights described in sect. 2.5 we have applied a weight to allow for the fact that the decay particles from a Λ^0 decay can have very low momenta and consequently be difficult to process. Minimum momentum cutoffs of 155 MeV/c and 55 MeV/c were applied to the decay proton and pion respectively and the accepted events were given a weight W where

$$W = \frac{2}{1 - \cos \theta}$$

and θ is that angle (between the proton or pion in the Λ^0 rest frame and the Λ^0 direction in the c.m. rest frame) which corresponds to the respective cutoff momentum in the laboratory [3]. The minimum momentum cutoff values were determined by the usual procedure of maximising the total number of weighted events by varying the cutoff values.

For the one- and two-prong events there is an additional weight to allow for the difficulty of scanning and processing events with a small laboratory angle between the incident kaon and outgoing pion. The azimuthal distribution of the outgoing pions about the beam direction revealed such a loss which was more serious for unseen spectator events. From the expected flatness of the azimuthal distribution, correction factors were derived as a function of c.m. scattering angle θ between the K^- and the π^- for events with seen and unseen spectators separately and for each experiment. Details of this procedure and the weights that were obtained are published elsewhere [5].

4. K^- and \bar{K}^0 channels

In this experiment the main K^- and \bar{K}^0 channels that have been studied are



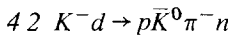
There is no serious ambiguity problem for these reactions and the numbers of fitted events are presented in table 4. No special weights were required but the presence of two nucleons in the final state leads to some difficulty in the identification of the spectator nucleon. This is discussed separately for reactions (6) and (7) in the next two sections.

4.1. $K^- d \rightarrow p K^- \pi^- p$

In this reaction because of the absence of a $K^- \pi^-$ isobar and the presence of a minimum momentum transfer to the target nucleon there are very few events with

two slow protons in the final state [4]. The spectator is taken as the slower proton and this yields the spectator momentum distribution shown in fig. 1a for experiment 2.

Superimposed on this data is a normalised curve corresponding to the predictions of the Hulthén wave function. This is in reasonable agreement with the data, as expected for this well constrained channel. Effects due to the Pauli exclusion principle are not expected to be important here because of the lack of events with two slow protons. This is in contrast with the two-body charge exchange reactions such as $K^+d \rightarrow K^0pp$ where the effect can be large [6]



This final state contains contributions from the reactions

- (a) $K^-d \rightarrow p_s\bar{K}^0\pi^-n$,
- (b) $K^-d \rightarrow n_s\bar{K}^0\pi^-p$,
- (c) $K^-d \rightarrow d\bar{K}^0\pi^-$ (misfitted),

as well as more complicated processes involving secondary interactions. In this channel there are many events where both nucleons have laboratory momenta less than 280 MeV/c and this makes the spectator identification difficult. Reaction (c) is more important at the higher momenta and for experiment 5 may be observed in fig. 3a as an enhancement at low pn effective masses, or in fig. 3b at values of $\hat{p} \cdot \hat{n}$ close to unity, where \hat{p} and \hat{n} are unit vectors along the proton and neutron directions respectively. Many of the events with two slow nucleons correspond to fast forward $\bar{K}^*(890)$ production, for which the minimum three-momentum acquired by an initially stationary target nucleon is at least 130 MeV/c even at the highest c.m. energies considered. Thus a reasonable separation between reactions (a) and (b) can be made by assuming the slower nucleon to be the spectator. For events with a very slow proton, including most of the unseen spectator events, the sample of reaction (a) is very pure. However, for fast protons there is an ambiguity between interpretations (a) and (b) which increases slightly with c.m. energy, and which is shown by the plot of neutron against proton momentum in fig. 3c. We estimate that the slower nucleon criterion leads to 1% of the events from channel (a) being assigned to channel (b). Finally the above selection also yields a sample of reaction (a) uncontaminated by reaction (c) as shown by the cross hatched histograms of figs. 3a and b. As the momentum of a proton of a given range is more than half that of a deuteron of the same range, if a seen spectator-like track is incorrectly fitted as a proton when really a deuteron, the fitted momentum of the unseen neutron is necessarily less than that of the proton. Thus the cut excludes the coherent deuteron events, which can be seen as a band on fig. 3c.

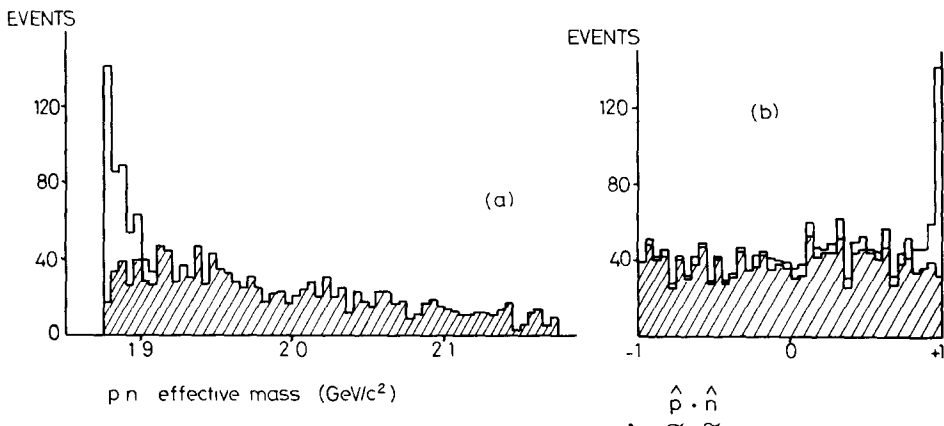


Fig. 3 (a) Effective mass distribution of the (pn) system for the events of reaction (7) from experiment 5 before the slower nucleon requirement was applied to the spectator proton. (b) Distribution of $\hat{p} \cdot \hat{n}$ for the same events as in 3a (In both cases the shaded distributions are for events where the proton is the slower nucleon)

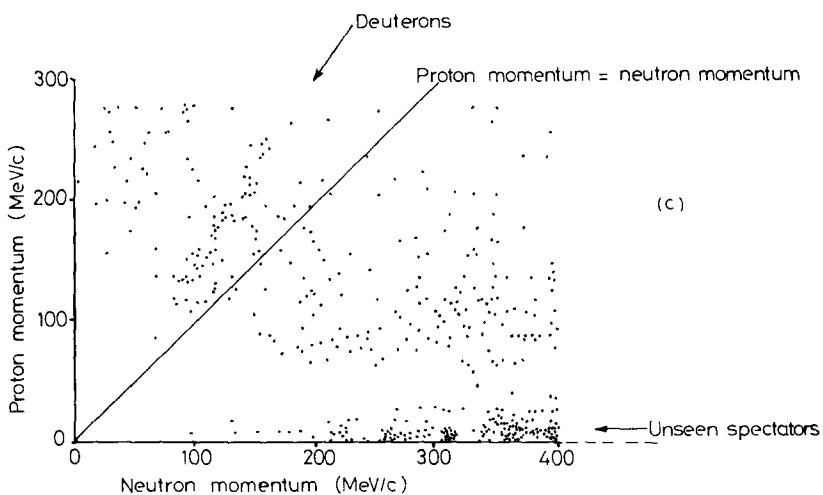


Fig. 3c. Scatter plot of neutron momentum versus proton momentum for reaction (7) events from experiment 5

5. Σ^- and Σ^+ channels

The reactions involving charged Σ decays which are described in this paper are listed in table 2. The numbers of fitted events in these channels are presented in table 4. There is very little kinematic overlap between these reactions, and as the predicted ionisation of the Σ was always compared with the observed bubble den-

sity we believe that there is no serious contamination from other fits. There is some difficulty in separating reaction (8) from the reaction $K^- d \rightarrow p_s \Sigma^- + \text{missing mass}$, and this is discussed later in this section.

In addition to the general weights described in sect. 2, we have applied an extra weight to the charged Σ channels to allow for the loss of events with a small projected laboratory angle between the charged Σ and the charged decay track. This is most serious in reactions (10b) and (12b) where ionisation change at the Σ^+ decay point is frequently small. This loss was studied by comparing the azimuthal distribution of the decay plane normal about the Σ direction with the expected isotropic distribution, for different ranges of laboratory decay angle. Losses were observed when the chamber optic axis lay close to the decay plane for events where the angle between the Σ and the charged decay track in the laboratory rest frame was less than 8° . All such events were rejected and a corrective weight was applied to the remainder, of the form

$$W = \frac{2}{1 + \cos \theta} ;$$

for each event θ is the angle in the rest frame of the Σ corresponding to the cutoff angle of 8° in the laboratory frame.

To reduce the contribution of multi-neutral reactions to the sample of reaction (8) we have followed a procedure which allocates a weight to each event as follows [7]

$$\left| \frac{m^2 - m_\pi^2}{\Delta(m^2)} \right| \leq 1, \quad \text{weight} = 1,$$

$$\frac{m^2 - m_\pi^2}{\Delta(m^2)} > 1, \quad \text{weight} = 0,$$

$$\frac{m^2 - m_\pi^2}{\Delta(m^2)} < -1, \quad \text{weight} = 2,$$

where m^2 and $\Delta(m^2)$ are the missing mass squared and error on missing mass squared for reaction (8) and m_π^2 is the neutral pion mass squared. As the genuine events should have a symmetric missing mass squared distribution, this weighting reduces the contamination from multi-neutral events. The use of $\Delta(m^2)$ in the selection procedure ensures that there is no bias against less well measured events such as those with a high momentum Σ .

6. Channel cross sections

These were calculated using the path lengths found from tau decays in each of the experiments. The 1130, 1320 and 1780 MeV/c experimental cross sections are

Table 5
Channel cross sections for each experiment

Experiment	1	2	3	4	5
Reaction					
(1) $K^-n \rightarrow \Lambda^0 \pi^-$	3.29 ± 0.20	2.19 ± 0.12	2.21 ± 0.18	2.00 ± 0.20	1.43 ± 0.10
(2) $K^-n \rightarrow \Lambda^0 \pi^- \pi^0$	3.67 ± 0.22	3.23 ± 0.18	3.59 ± 0.26	2.62 ± 0.24	2.56 ± 0.18
(3) $K^-n \rightarrow \Sigma^0 \pi^-$	1.07 ± 0.07	0.75 ± 0.05	0.47 ± 0.06	0.52 ± 0.13	0.44 ± 0.03
(4) $K^-n \rightarrow \Lambda^0 \pi^+ \pi^- \pi^-$	0.22 ± 0.02	0.33 ± 0.03	0.57 ± 0.06	0.86 ± 0.10	0.60 ± 0.05
(5) $K^-n \rightarrow \Sigma^0 \pi^+ \pi^- \pi^-$	0.03 ± 0.01	0.06 ± 0.01	—	—	0.22 ± 0.02
(6) $K^-n \rightarrow K^- \pi^- p$	0.86 ± 0.05	0.90 ± 0.07	1.50 ± 0.11	2.01 ± 0.17	1.59 ± 0.11
(7) $K^-n \rightarrow K^0 \pi^- n$	1.65 ± 0.10	2.02 ± 0.15	2.86 ± 0.22	3.10 ± 0.30	3.02 ± 0.21
(8) $K^-n \rightarrow \Sigma^- \pi^0$	0.98 ± 0.07	0.80 ± 0.06	0.48 ± 0.05	0.46 ± 0.06	0.44 ± 0.03
(9) $K^-n \rightarrow \Sigma^- \pi^+ \pi^-$	0.67 ± 0.04	0.66 ± 0.05	0.76 ± 0.07	0.79 ± 0.08	0.63 ± 0.05
(10) $K^-n \rightarrow \Sigma^+ \pi^- \pi^-$	1.13 ± 0.08	0.86 ± 0.05	1.03 ± 0.07	0.70 ± 0.07	0.72 ± 0.05
(11) $K^-n \rightarrow \Sigma^- \pi^+ \pi^- \pi^0$	0.07 ± 0.01	0.13 ± 0.01	0.26 ± 0.03	0.51 ± 0.06	0.52 ± 0.04
(12) $K^-n \rightarrow \Sigma^+ \pi^- \pi^- \pi^0$	0.06 ± 0.01	0.09 ± 0.01	0.13 ± 0.02	0.16 ± 0.02	0.18 ± 0.02

presented here for the first time. The cross sections from the 1450 and 1650 MeV/c experiments have been previously published [1] but are included here for completeness. The new data have been corrected for several effects as follows

- (i) Scanning and processing efficiencies for each topology.
- (ii) Neutral decays of strange particles, decays outside the chamber and decays close to the production vertex.
- (iii) The channel averaged fractions of events having a spectator proton momentum greater than 280 MeV/c were determined on samples of data from experiments 3 and 4 [1]. These factors have also been used to correct for unobserved fast spectator events in experiments 1, 2 and 5.
- (iv) The Glauber screening of the neutron in the target deuteron gives rise to correction factors of 1.08, 1.055 and 1.06 for experiments 1, 2 and 5 respectively. The data have also been corrected for specific losses in individual channels as described in the preceding sections.

The channel cross sections for each of the experiments are listed in table 5. Owing to the motion of the neutron within the deuteron each experiment does not correspond to a unique c.m. energy. In the next section the energy dependence of the cross section is extracted for those reactions with sufficient events for the unfolding procedure.

The cross sections of reactions (3) and (8) should be identical apart from small kinematic factors, and within experimental errors this is the case. The only further internal consistency checks that can be applied to the cross sections involve quasi-two-body processes which can be related in different channels through known resonance branching fractions. We have applied these checks where possible and find reasonable agreement. However, as the isolation of such processes is always model dependent we believe that such comparisons should be treated with caution.

7. Cross-section variation with energy

Assuming the validity of the impulse approximation [8], the c.m. energy E of the K^- neutron system for each event is equal to the effective mass of all the secondaries except the spectator proton. The selected sample of events has a continuous distribution in energy ranging from 1750 to 2200 MeV. To unfold the neutron cross section $\sigma(E)$ at energy E from the observed number of events $N(E) dE$ in an interval dE about E we have used the relation

$$N(E) dE = E \sigma(E) dE \int \frac{B(p) dp}{p} \int_{p_1}^{p_2} |\Phi_H(p_s)|^2 F(p_s) p_s dp_s .$$

The left-hand side is determined experimentally and the right-hand side can be calculated but for the factor $\sigma(E)$. Comparison of the two yields this latter quantity, p is the beam momentum and $B(p)$ is the distribution of beam momentum, assumed

Table 6
Cross sections for each reaction as a function of c.m. energy

Reaction number	(1)	(2)	(3)	(4)
Reaction	$K^-n \rightarrow \Lambda^0 \pi^-$	$K^-n \rightarrow \Lambda^0 \pi^- \pi^0$	$K^-n \rightarrow \Sigma^0 \pi^-$	$K^-n \rightarrow \Lambda^0 \pi^- \pi^+ \pi^-$
c.m. energy interval				
1750–1780	5.58 ± 0.49	3.89 ± 0.60	1.72 ± 0.26	0.26 ± 0.06
1780–1810	4.80 ± 0.34	3.79 ± 0.42	1.35 ± 0.18	
1810–1840	2.85 ± 0.23	3.34 ± 0.37	0.81 ± 0.14	
1840–1870	2.50 ± 0.18	2.86 ± 0.27	0.80 ± 0.11	0.21 ± 0.03
1870–1900	2.43 ± 0.19	3.70 ± 0.29	1.09 ± 0.12	
1900–1930	2.17 ± 0.17	3.35 ± 0.29	0.67 ± 0.10	0.23 ± 0.03
1930–1960	1.82 ± 0.15	3.10 ± 0.30	0.53 ± 0.09	
1960–1990	2.01 ± 0.16	3.84 ± 0.33	0.32 ± 0.06	0.31 ± 0.04
1990–2020	2.30 ± 0.18	3.59 ± 0.35	0.40 ± 0.09	0.73 ± 0.09
2020–2050	2.23 ± 0.17	3.37 ± 0.29	0.67 ± 0.09	0.70 ± 0.10
2050–2080	1.99 ± 0.18	2.84 ± 0.26	0.42 ± 0.09	0.70 ± 0.09
2080–2110	1.60 ± 0.15	2.47 ± 0.27	0.59 ± 0.11	0.69 ± 0.09
2110–2140	1.40 ± 0.13	2.49 ± 0.27	0.58 ± 0.10	0.57 ± 0.09
2140–2170	1.16 ± 0.13	2.55 ± 0.31	0.69 ± 0.14	0.68 ± 0.09
2170–2200	1.15 ± 0.14	2.54 ± 0.31	0.38 ± 0.10	0.72 ± 0.09

to be Gaussian for all exposures. $\Phi_H(p_s)$ is the Fourier transform of the Hulthén wave function for the deuteron and $F(p_s)$ is a flux factor [9]. To obtain $N(E) dE$ when using the above relation, events from all exposures were combined and correspondingly the factor $B(p)$ allowed for the various beam momenta and their different millibarn equivalents. In our study of the energy dependence of the cross sections we use a restricted sample of events corresponding to that interval of spectator momentum which is well fitted by the Hulthén wave function. The interval used, from $p_1 = 90$ to $p_2 = 240$ MeV/c, was determined from plots such as those in fig. 1. The tails of the energy distribution for each experiment were excluded because of low statistics and because the high-energy tails include fast, forward spectators which are more likely to result from secondary interactions.

The events were divided into 30 MeV c.m. energy bins, except that for reaction (4) some low statistics bins have been combined, and the theoretical curve was integrated over each bin. In every reaction as a consistency check the procedure was applied for each experiment separately. As an example the results for reaction (9) are shown in fig. 4 for each experiment separately. There is good agreement between the experiments for this reaction and most of the others. Reactions (6) and (7) are less consistent as might be expected because these are the reactions where the identification of the spectator is most difficult. For reaction (7) we have restricted the spectator proton momentum range to 90–140 MeV/c in order to further reduce the

(6)	(7)	(8)	(9)	(10)
$K^- n \rightarrow K^- \pi^- p$	$K^- n \rightarrow \bar{K}^0 \pi^- n$	$K^- n \rightarrow \Sigma^- \pi^0$	$K^- n \rightarrow \Sigma^- \pi^+ \pi^-$	$K^- n \rightarrow \Sigma^+ \pi^- \pi^-$
0.90 ± 0.13		1.16 ± 0.19	0.85 ± 0.14	1.40 ± 0.19
0.95 ± 0.10	1.49 ± 0.23	0.89 ± 0.13	0.69 ± 0.09	1.18 ± 0.12
0.80 ± 0.08	1.38 ± 0.22	1.13 ± 0.14	0.72 ± 0.08	1.41 ± 0.13
0.73 ± 0.07	1.53 ± 0.19	0.89 ± 0.10	0.56 ± 0.07	0.94 ± 0.09
0.82 ± 0.06	1.86 ± 0.20	0.96 ± 0.10	0.61 ± 0.06	0.85 ± 0.07
0.91 ± 0.08	2.04 ± 0.23	0.77 ± 0.10	0.62 ± 0.07	0.99 ± 0.10
1.03 ± 0.09	2.00 ± 0.23	0.50 ± 0.08	0.70 ± 0.07	0.81 ± 0.09
1.41 ± 0.11	2.47 ± 0.27	0.58 ± 0.09	0.89 ± 0.09	1.00 ± 0.10
1.45 ± 0.13	2.80 ± 0.34	0.44 ± 0.09	0.71 ± 0.07	1.07 ± 0.11
1.76 ± 0.13	3.50 ± 0.33	0.48 ± 0.07	0.67 ± 0.07	0.76 ± 0.09
1.80 ± 0.16	3.42 ± 0.35	0.76 ± 0.13	0.79 ± 0.08	0.99 ± 0.11
1.81 ± 0.16	2.84 ± 0.32	0.49 ± 0.09	0.66 ± 0.08	0.59 ± 0.08
1.67 ± 0.16	2.73 ± 0.31	0.45 ± 0.09	0.69 ± 0.08	0.51 ± 0.07
1.56 ± 0.15	3.01 ± 0.33	0.49 ± 0.12	0.56 ± 0.07	0.54 ± 0.07
1.75 ± 0.16	3.53 ± 0.39	0.40 ± 0.11	0.58 ± 0.08	0.61 ± 0.08

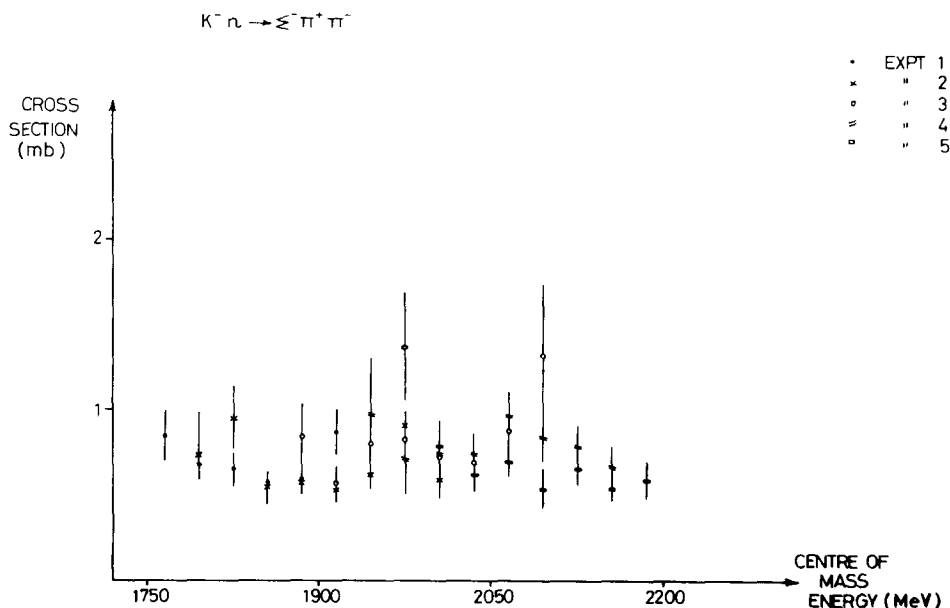


Fig. 4. Energy-dependent cross section for reaction (9) for experiments 1 to 5 separately.

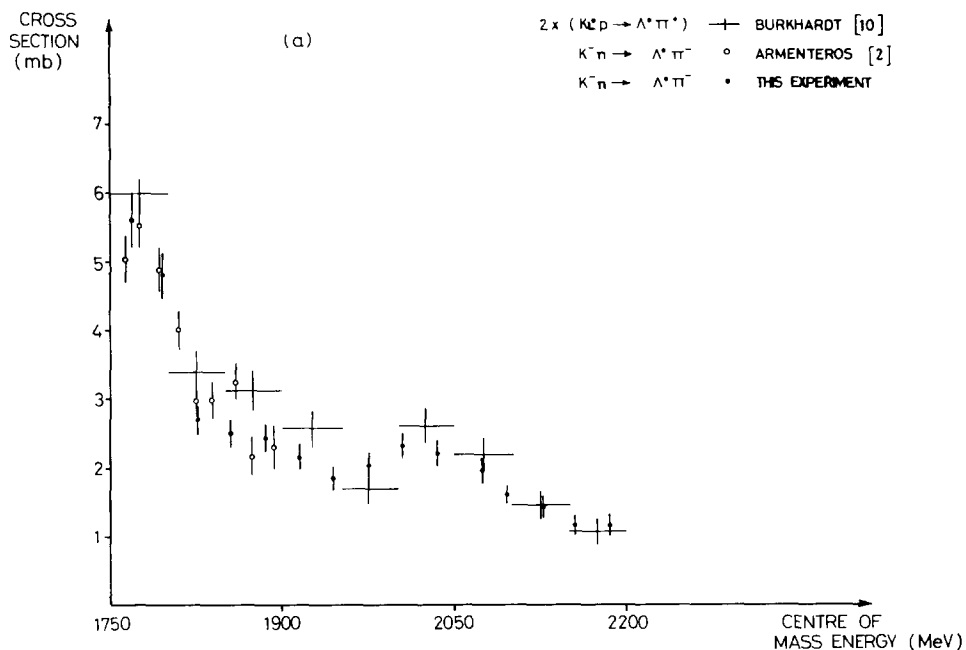


Fig. 5a. Energy-dependent cross section for reaction (1) together with comparable data from refs [2,10]

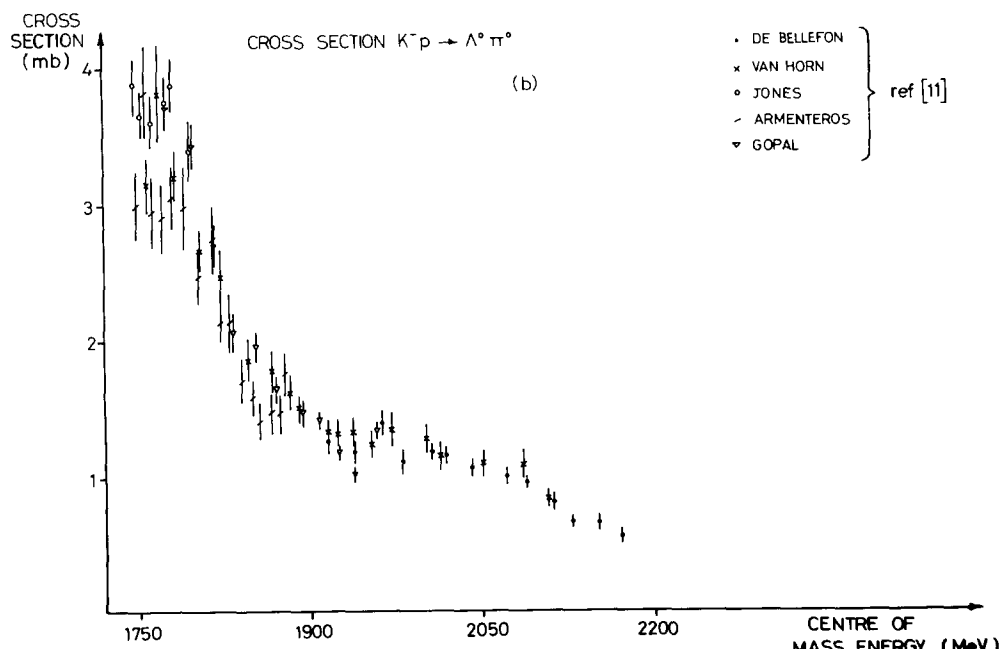


Fig. 5b. Cross sections for the reaction $K^- p \rightarrow \Lambda^0 \pi^0$ from refs. [11].

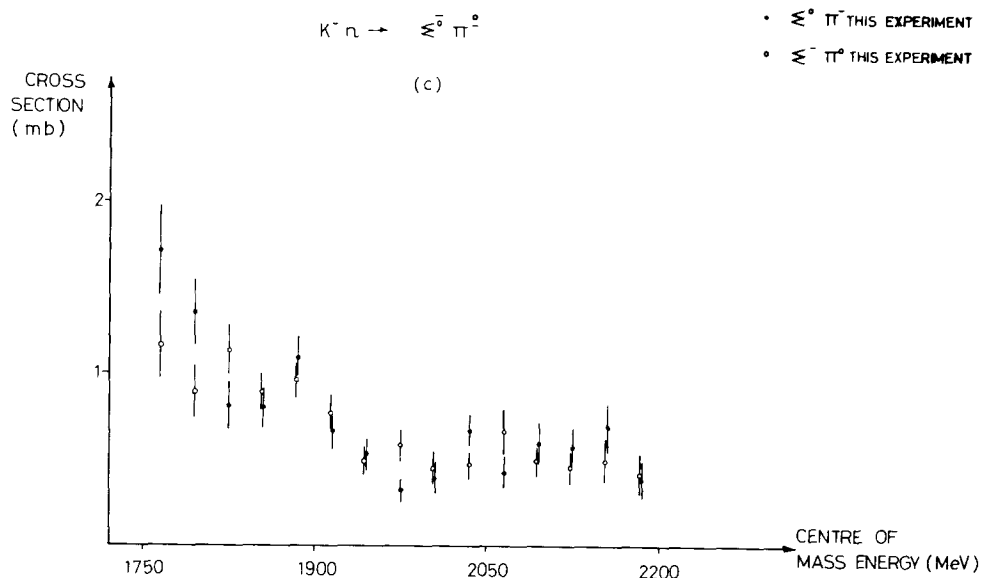


Fig 5c Energy-dependent cross sections for reactions (3) and (8)

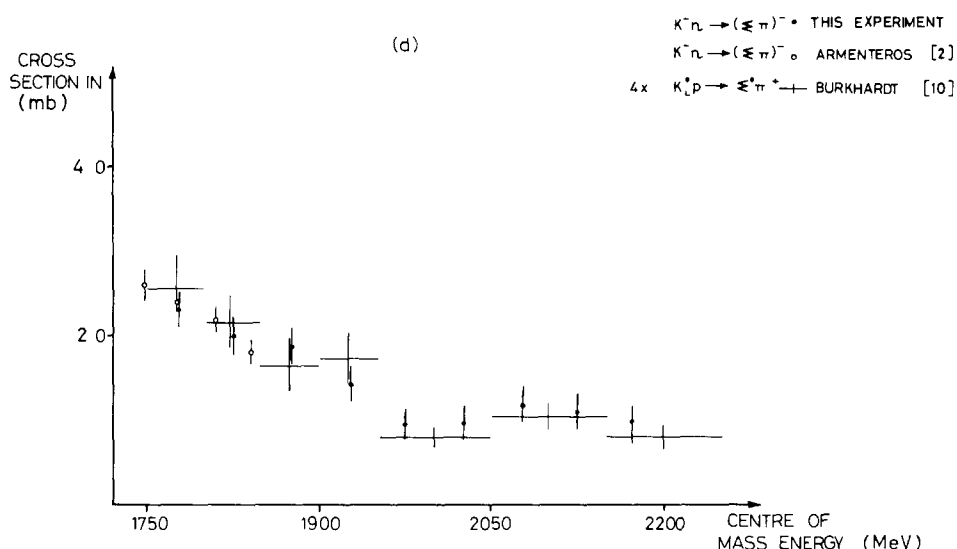


Fig 5d Energy-dependent cross sections for reactions (3) and (8) combined Comparable data from refs. [2,10] are shown on this and all later figures where it is available

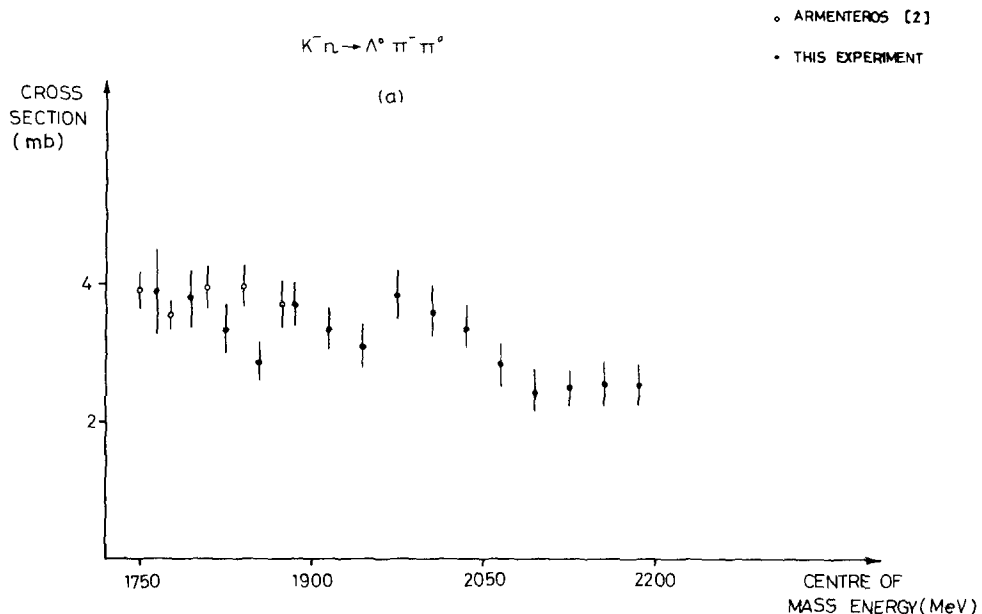


Fig. 6a. Energy-dependent cross sections for reaction (2).

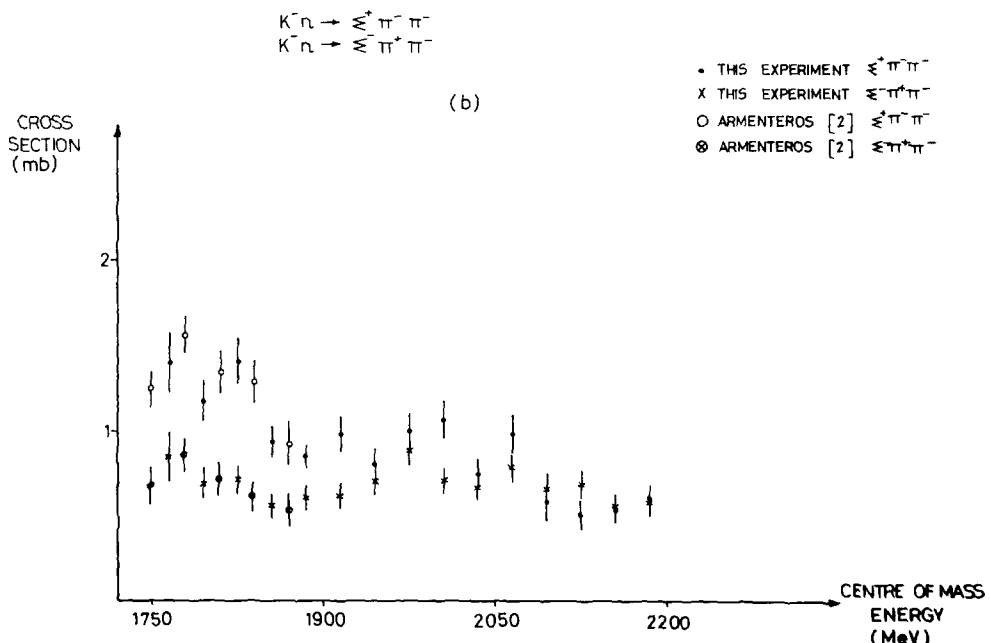


Fig. 6b Energy-dependent cross sections for reactions (9) and (10).

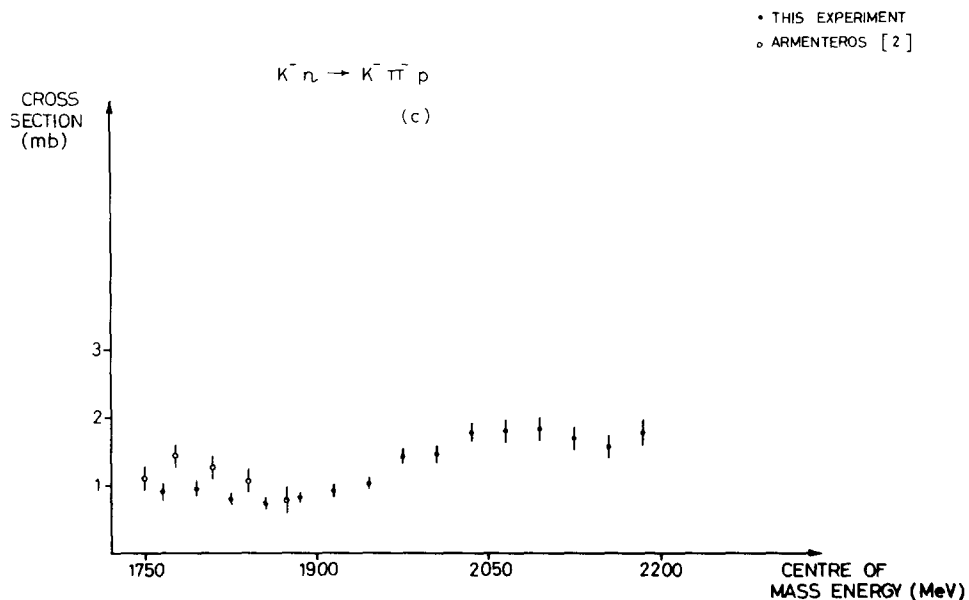


Fig. 6c Energy-dependent cross sections for reaction (6)

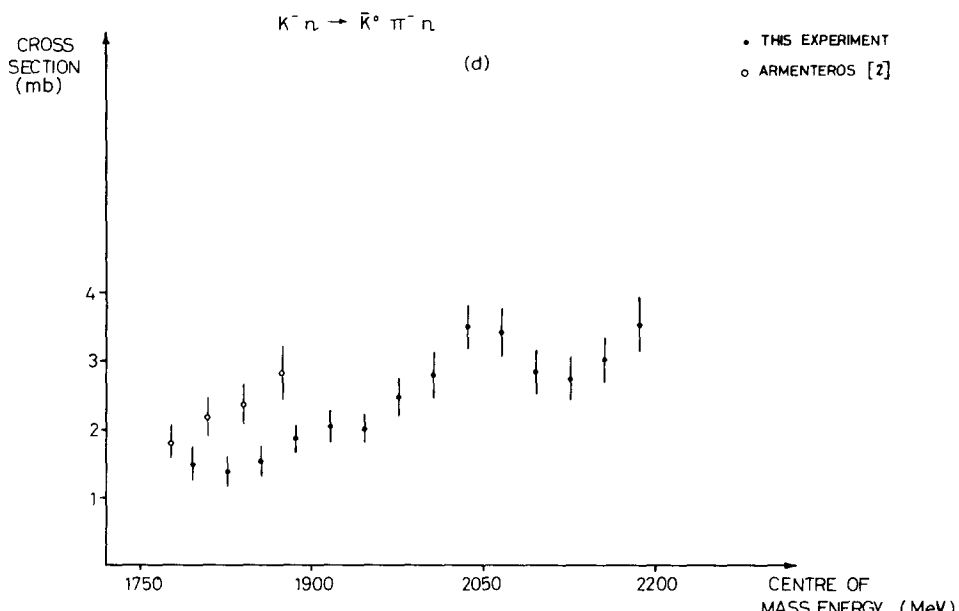


Fig. 6d. Energy-dependent cross sections for reaction (7).

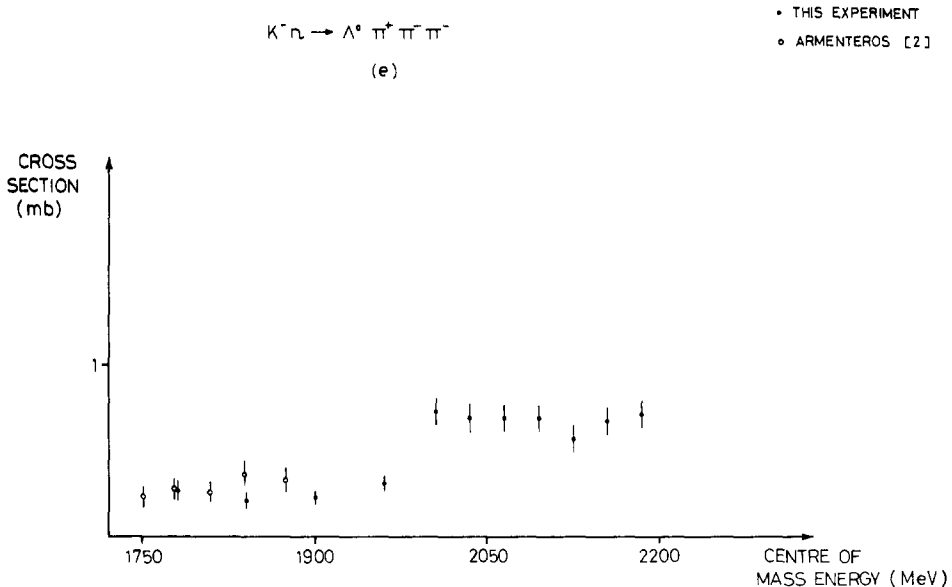


Fig. 6e Energy-dependent cross sections for reaction (4)

contribution of any neutron spectator events. The extracted cross sections for all the reactions are shown in table 6.

7.1 Results and conclusions

The energy-dependent cross section obtained for reaction (1) in these experiments is shown on fig. 5a together with the results of an overlapping K^- deuterium experiment [2] in which tau normalisation was also used. Also shown is the cross section from the only published results on the reaction $K_L^0 p \rightarrow \Lambda^0 \pi^+$ in our energy region [10]. There is good agreement between all of these experiments. There are many published cross section results on the reaction $K^- p \rightarrow \Lambda^0 \pi^0$ [11] (fig. 5b), and while these are internally consistent over most of our energy range, there are large differences below 1800 MeV resulting in an uncertainty of approximately 2 mb for reaction (1) in this region. (The $K^- p$ cross sections need to be multiplied by an isospin factor of two in order to compare with reaction (1)). The energy dependence of the cross section observed for reaction (1) in this experiment is in good agreement with that obtained from the equivalent $K^- p$ reaction. This reaction provides a useful check for the significance of the results that we present in the other channels. The magnitude of the cross section for reaction (1) observed in these deuterium experiments is systematically lower than the equivalent $K^- p \rightarrow \Lambda^0 \pi^0$ data for c.m. energies below 2000 MeV, where the effect of secondary interactions is more important. The authors of ref. [2] normalized their cross section for reaction (1) to the currently

available cross section data for the reaction $K^- p \rightarrow \Lambda^0 \pi^0$ and quoted appropriately normalised cross sections for the remaining channels. We prefer to quote our tau based cross sections for all channels because of the remaining uncertainty in the $K^- p \rightarrow \Lambda^0 \pi^0$ cross section. We point out, however, that the relatively small normalisation factors used in ref. [2] are similar in magnitude to the correction factors that we have applied to allow for the loss of events with proton momentum greater than 280 MeV/c, many of which may result from secondary interactions. Hence we show for comparison the cross sections from ref. [2] together with our own data on figs. 5 and 6.

The cross sections of reactions (3) and (8) are shown separately on fig. 5c. These reactions should have the same energy dependence and total cross sections within small kinematic factors. Consistent results are obtained even though these reactions involve quite different topologies, weights and treatment of ambiguities. We have repeated the procedure for these combined reactions to obtain the overall $K^- n \rightarrow (\Sigma\pi)^-$ cross section from our experiment which is shown in fig. 5d together with comparable data from refs. [2,10]. These both agree well with our data. The $\Sigma(1765)$ dominates this figure with no other striking resonance peaks in the cross section.

The cross section for reaction (2) is shown on fig. 6a. The data agree well with that from ref. [2]. Fig. 6b contains the cross section for reactions (9) and (10). Again the agreement is good and both experiments indicate a large difference in cross section between these reactions below an energy of 1900 MeV. At higher energies there is very little difference in the reaction cross sections. These reactions are dominated by the same quasi two-body final states, e.g. $\Lambda(1405)\pi$ and $\Lambda(1520)\pi$. The large difference in cross section at low energy could be due to strong interference between the crossing resonance bands on the Dalitz plot. This is more likely to occur in reaction (10) because of the presence of two negative pions in the final state leading to two possible Y^* combinations.

The cross sections for reactions (6) and (7) are shown on figs. 6c and 6d. In channel (7) in this experiment a restricted spectator momentum interval of 90 to 140 MeV/c has been used in order to minimize overlap with the $\bar{K}^0 \pi^- p n_s$ final state prior to imposing the slower nucleon spectator selection. This also reduces secondary interaction effects, which, it has been suggested, may be more important for channels with a kaon in the final state [12].

Finally, the cross section for reaction (4) is shown on fig. 6e. The two experiments agree well and there is a clear increase in cross section around 2000 MeV which we attribute to the strong $\Lambda(1815)\pi$ coupling of the $\Sigma(2030)$ [13].

The authors would like to thank the scanning and measuring staff at Birmingham University for their conscientious work and the Science Research Council for their support. We would also like to express our thanks to the Imperial College, Glasgow University and Edinburgh University groups for permission to use data from the 1450 and 1650 MeV/c experiments which were performed in collaboration.

References

- [1] D.C Colley *et al.*, Nucl Phys. B31 (1971) 61
- [2] R Armenteros *et al.*, Nucl Phys B18 (1970) 425
- [3] A J Van Horn, L B.L. thesis LBL-1370 (1972).
- [4] M J Corden, University of Birmingham thesis (1974)
- [5] M J Corden *et al* , Nucl Phys B104 (1976) 382.
- [6] D Cline, J Penn and D D Reeder, Nucl. Phys B22 (1970) 476.
- [7] A. Berthon *et al.*, Nucl. Phys B20 (1970) 476
- [8] G F Chew, Phys Rev 80 (1950) 196
- [9] G F. Cox *et al.*, Nucl. Phys. B19 (1970) 61
- [10] E Burkhardt *et al.*, Nucl. Phys. B99 (1975) 365
- [11] R. Armenteros *et al* , Nucl Phys B8 (1968) 233;
M Jones *et al.*, Nucl. Phys. B90 (1975) 349,
A. Van Horn *et al.*, Phys. Rev D6 (1972) 1275;
A. De Bellefon *et al* , Nuovo Cim. 7A (1972) 567,
G Gopal *et al.*, Nucl Phys B105 (1976) 189
- [12] D Pearce, Imperial College, London, thesis HEP/T/12 (1970)
- [13] M J. Corden *et al* , Nucl Phys B92 (1975) 365